

NASA TECHNICAL NOTE



NASA TN D-4788

NASA TN D-4788

LOAN COPY: RETURN
AFWL (WLIL-2)
KIRTLAND AFB, N M

0131389



TECH LIBRARY KAFB, NM

LAMINARIZATION OF A TURBULENT
BOUNDARY LAYER AS OBSERVED FROM
HEAT-TRANSFER AND BOUNDARY-LAYER
MEASUREMENTS IN CONICAL NOZZLES

*by Donald R. Boldman, James F. Schmidt,
and Anne K. Gallagher*

*Lewis Research Center
Cleveland, Ohio*



0131389

NASA TN D-4788

LAMINARIZATION OF A TURBULENT BOUNDARY LAYER AS OBSERVED
FROM HEAT-TRANSFER AND BOUNDARY-LAYER
MEASUREMENTS IN CONICAL NOZZLES

By Donald R. Boldman, James F. Schmidt, and Anne K. Gallagher
Lewis Research Center
Cleveland, Ohio

NATIONAL AERONAUTICS AND SPACE ADMINISTRATION

For sale by the Clearinghouse for Federal Scientific and Technical Information
Springfield, Virginia 22151 - CFSTI price \$3.00

ABSTRACT

Heat-transfer measurements were obtained in 30° and 60° half-angle of convergence nozzles at a nominal stagnation temperature of 970°R (539 K) and over a range of stagnation pressures of 2.0 to 20.4 atmospheres (2.03×10^5 to $20.67 \times 10^5\text{ N/m}^2$). These conditions provided nozzle-throat Reynolds numbers based on diameter of about 6.0×10^5 to 5.0×10^6 . Boundary-layer time-mean velocity and temperature measurements were obtained at one station in a water-cooled pipe inlet and at a subsonic (Mach number ≤ 0.08) station in each nozzle at stagnation pressures of 3.1 and 20.4 atmospheres (3.14×10^5 and $20.67 \times 10^5\text{ N/m}^2$). The heat-transfer and boundary-layer surveys suggested the occurrence of laminarization of an initially turbulent boundary layer.

LAMINARIZATION OF A TURBULENT BOUNDARY LAYER AS OBSERVED FROM HEAT-TRANSFER AND BOUNDARY-LAYER MEASUREMENTS IN CONICAL NOZZLES

by Donald R. Boldman, James F. Schmidt, and Anne K. Gallagher

Lewis Research Center

SUMMARY

Heat-transfer measurements were obtained in 30° and 60° half-angle of convergence nozzles at a nominal stagnation temperature of 970°R (539K) and over a range of stagnation pressures of about 2.0 to 20.4 atmospheres (2.03×10^5 to $20.67 \times 10^5\text{N/m}^2$). These conditions provided nozzle-throat Reynolds numbers based on diameter of about 6.0×10^5 to 5.0×10^6 . Time-mean boundary-layer velocity and temperature measurements were obtained at one station in a water-cooled pipe inlet and at a subsonic (Mach number ≤ 0.08) station in each nozzle at stagnation pressures of 3.1 and 20.4 atmospheres (3.14×10^5 and $20.67 \times 10^5\text{N/m}^2$). At these pressure levels, the thermal and velocity boundary layers in the pipe inlet were conventional for turbulent pipe flow.

The heat transfer at a given station in the nozzles generally exhibited two distinct depressions from the predicted levels based on a turbulent pipe flow type of correlation. The larger of these depressions occurred at lower Reynolds numbers and was assumed to be the result of laminarization of the initially turbulent boundary layer. The smaller of these depressions, which occurred at higher Reynolds numbers, was assumed to be the result of reduced turbulent transport associated with a turbulent boundary layer in an accelerating flow.

A time-mean boundary-layer velocity profile was obtained in each nozzle at one set of conditions in the low Reynolds number range. These profiles were described by a power law which is often associated with laminar flow. Although absolute confirmation of laminarization cannot be established on the basis of time-mean surveys, the laminar-type velocity profile provides evidence in support of the laminarization postulate. In progressing towards the throat of each nozzle, the heat transfer at the low Reynolds number condition approached a classical laminar flow level, thus lending additional support to the feasibility of laminarization.

A critical value of the acceleration parameter was derived from the integral momentum equation for axisymmetric flow assuming flat-plate boundary-layer transition criteria and an empirical relation for the shear stress, form factor, and velocity gradient. The critical acceleration parameter, which was within the range of values reported by others, provided a fair definition of the regions of low and high depressions in the heat transfer in the two nozzles.

INTRODUCTION

Experimental investigations of nozzle heat transfer have revealed that the throat heat flux is generally lower than the levels in a pipe of the same diameter and mass flow. In reference 1 it was shown that the magnitude of the depression in throat heat flux for a given nozzle varied with the Reynolds number. These depressions in heat flux were attributed to the reduction of turbulence which accompanies highly accelerated turbulent flows. In a rather limited range of conditions the acceleration of the flow is believed to bring about laminarization of the boundary layer and, consequently, large reductions in the heat transfer may be expected.

The subject of laminarization of a turbulent boundary layer has been discussed, for instance, in references 1 to 7. In the majority of these references the allusion to a laminar boundary layer was established by means of heat-transfer measurements and/or time-mean boundary-layer surveys. The word "laminarization," in this sense, refers to the transition of a turbulent boundary layer to one which possesses time-mean laminar characteristics or contributes to a transport of heat which is approximately predictable by classical zero pressure gradient type laminar boundary-layer correlations. This connotation of the word laminarization will also be applied to the present investigation; however, it should be emphasized that time-mean profiles and heat-transfer data provide only a superficial understanding of the boundary layer. Assessment of the true character of the boundary layer would, of course, require the measurement of changes in turbulence structure and intensity, which is beyond the scope of this report.

The current investigation was conducted primarily to provide further evidence of the phenomenon of laminarization resulting from the flow acceleration induced by conical nozzles. In view of this objective, heat-transfer measurements were obtained in 30° and 60° half-angle of convergence nozzles at a nominal stagnation temperature of 970° R (539 K) and over a stagnation-pressure range of about 2.0 to 20.4 atmospheres (2.03×10^5 to 20.67×10^5 N/m²). These conditions permitted development of a time-mean turbulent hydrodynamic and thermal boundary layer in a water-cooled pipe inlet which was coupled to the nozzles. Boundary-layer surveys of temperature and velocity were obtained at one station in the inlet and at a subsonic station in each nozzle, at stagnation pressures of 3.1 and 20.4 atmospheres (3.14×10^5 and 20.67×10^5 N/m²).

A second objective of the investigation was to establish and evaluate in terms of the experimental heat transfer a critical value of the acceleration parameter of the type discussed in reference 3. The purpose of this acceleration parameter was to categorize the extent of the acceleration effects on the heat-transfer characteristics of an initially turbulent flow. The critical value of the acceleration parameter was determined from the integral momentum equation in order to establish an upper bound for the conditions in which reductions in heat transfer through laminarization might be experienced. The in-

tegral momentum equation contained certain empiricisms which differed from those of reference 3 but presumably were more compatible with the accelerating flow in conical nozzles.

SYMBOLS

A	area
C_1, C_2, C_3	constants
D	diameter
H	boundary-layer form factor, $H = \delta^*/\theta$
i	enthalpy
K	acceleration parameter
M	Mach number
P	pressure
Pr	Prandtl number
q	local heat flux
Re	Reynolds number
r	radius
St	Stanton number
T	temperature
t	temperature on heat-flux meter
u	velocity
x	distance along wall
Y	distance along heat-flux meter measured from gas-side wall
y	distance normal to the wall
z	axial coordinate measured from inlet boundary-layer survey station
Γ	velocity-gradient parameter given by eq. (B4)
Δ	thermal boundary-layer thickness
δ	velocity boundary-layer thickness

δ^* compressible boundary-layer displacement thickness, $\delta^* = \int_0^\infty \left(1 - \frac{\rho u}{\rho_\infty u_\infty}\right) dy$

ϵ shear-stress parameter given by eq. (B3)

θ compressible boundary-layer momentum thickness, $\theta = \int_0^\infty \frac{\rho u}{\rho_\infty u_\infty} \left(1 - \frac{u}{u_\infty}\right) dy$

μ dynamic viscosity

ν kinematic viscosity

ρ density

τ shear stress

Subscripts:

ad adiabatic wall condition

ax axisymmetric

c curvature of nozzle throat

cr critical value establishing boundary-layer transition

D based on diameter

i inlet

pf turbulent pipe flow

ref reference enthalpy condition

s freestream static condition

t local stagnation condition

w wall condition

θ based on momentum thickness

∞ freestream

0 stagnation condition

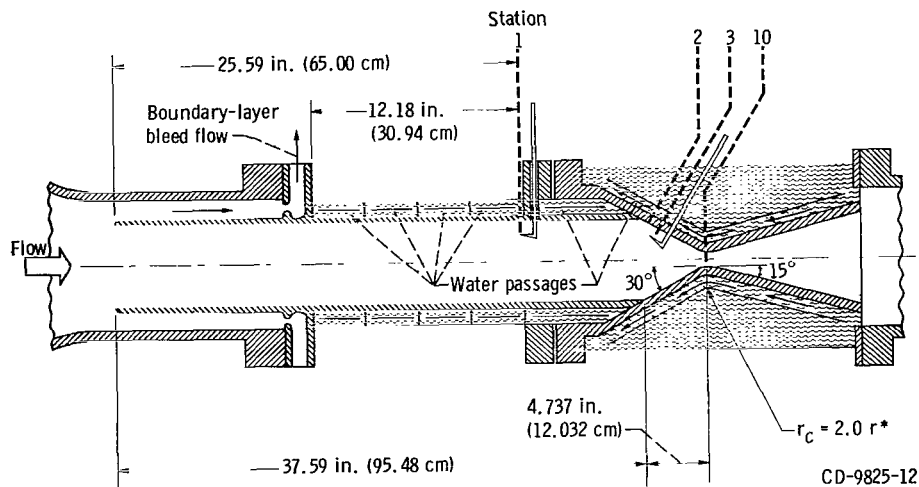
Superscript:

* geometric throat of nozzle

APPARATUS AND INSTRUMENTATION

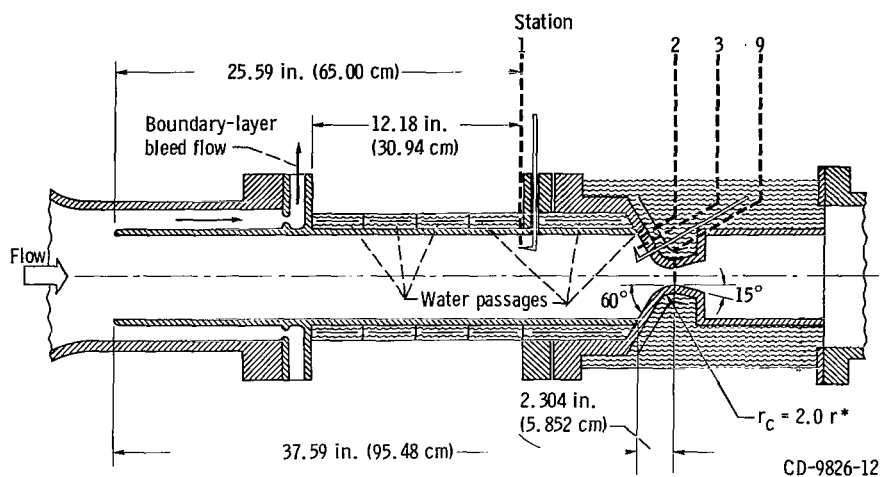
The heat-transfer facility, boundary-layer probes, heat-flux meters, and nozzles used in this investigation have been described in references 8 to 10. An important difference between the hardware used in the present study and that previously reported concerns the pipe inlet configuration. The inlets used in the experiments of references 8 to 10 were uncooled; however, in the present investigation a water-cooled inlet was used. Pertinent details of the design of the inlet, as well as a condensed description of the previously reported apparatus and instrumentation, are presented herein.

The test configurations consisted of a 6.5-inch-diameter (16.5-cm-diam) by 37.59-inch-long (95.48-cm-long) pipe inlet coupled to water-cooled 30° and 60° half-angle of convergence by 15° half-angle of divergence conical nozzles as shown in figures 1 and 2, respectively. Hereinafter, these nozzles will be identified by their convergence half-



Station	Area ratio, A/A^*	Diameter, D		Axial distance, z	
		in.	cm	in.	cm
1	18.98	6.50	16.51	0	0
2	11.648	5.092	12.934	13.218	33.574
3	6.952	3.934	9.992	14.221	36.121
4	5.591	3.528	8.961	14.575	37.021
5	4.395	3.128	7.945	14.921	37.899
6	3.328	2.722	6.914	15.273	38.793
7	2.410	2.316	5.883	15.623	39.682
8	1.392	1.760	4.470	16.120	40.945
9	1.024	1.510	3.835	16.558	42.057
10	1.000	1.492	3.790	16.733	42.502

Figure 1. - Nozzle configuration and instrumentation sites for 30° nozzle.



Station	Area ratio, A/A^*	Diameter, D		Axial distance, z	
		in.	cm	in.	cm
1	18.80	6.50	16.51	0	0
2	9.352	4.584	11.643	12.548	31.872
3	7.769	4.178	10.612	12.665	32.169
4	6.299	3.762	9.555	12.785	32.474
5	3.322	2.732	6.939	13.094	33.259
6	2.373	2.309	5.865	13.280	33.731
7	1.341	1.736	4.409	13.719	34.846
8	1.023	1.516	3.851	14.154	35.951
9	1.000	1.499	3.807	14.300	36.322

Figure 2. - Nozzle configuration and instrumentation sites for 60° nozzle.

angles only. Air, heated to a nominal stagnation temperature of 970⁰ R (539 K), entered the inlet at controlled stagnation pressures ranging from 2.0 to 20.4 atmospheres (2.03×10^5 to 20.67×10^5 N/m²). A plenum boundary-layer bleed system was used to establish a uniform velocity profile upstream of the inlet.

The inlet was fabricated from AISI 304 stainless-steel pipe which was machined to a wall thickness of 0.25 inch (0.64 cm). Cooling of the inlet commenced 13.41 inches (34.06 cm) from the leading edge and was maintained over the remaining length of 24.18 inches (61.42 cm). A boundary-layer survey station was located 12.00 inches (30.48 cm) upstream of the nozzle entrance. Inlet wall temperatures were determined from Chromel-Alumel thermocouple plugs which were threaded into the wall.

In discussion of the experimental nozzle heat flux, reference will be made to a second water-cooled inlet having a diameter of 3.1 inches (7.87 cm) and a cooled length of about 18 inches (45.72 cm). The purpose of this inlet was to determine the influence of contraction area ratio on the throat heat transfer in order to compare the results of this

investigation with the experiment of reference 11. Such a comparison was desirable since the nozzle used in reference 11 was geometrically similar to the present nozzle, and operating conditions were nearly the same. The method of heat-flux measurement in reference 11 differed from that of the present experiment.

The heat-transfer data in this investigation were obtained at nine measuring stations in the 30° nozzle and at eight stations in the 60° nozzle (refer to figs. 1 and 2, respectively). An Inconel heat-flux meter of the type described in reference 8 and a wall static pressure tap were located at each station in the nozzle. The 30° nozzle contained a boundary-layer survey station with an area ratio of 6.952 (station 3), which corresponds to a Mach number of about 0.08. A boundary-layer survey station with an area ratio of 7.769 (station 3) was located in the 60° nozzle. The Mach number at the 60° nozzle survey station was nominally 0.05 (based on the experimental pressure ratio and isentropic flow).

The boundary-layer kinetic-head measurements were obtained with a pitot probe having a rectangular opening 0.002 inch (0.0051 cm) high by 0.030 inch (0.0762 cm) wide. The boundary-layer temperature profile was measured in the plane of the kinetic-head measurements by means of a probe containing a bare-junction Chromel-Alumel thermocouple. The diameter of the junction was 0.005 inch (0.0127 cm). References 7 and 8 should be consulted for further details concerning the design of the boundary-layer probes.

The pressure and temperature probes were driven in a direction normal to the wall by precision motorized actuators geared to linear potentiometers. Probe contact with the wall was established by means of an electrical short circuit. A ± 0.1 -percent linearity of the potentiometers allowed for position measurements within ± 0.002 inch (± 0.0051 cm) for the temperature probes and the inlet pressure probe. Based on the actuator linearity, position measurements for the pressure probe in each nozzle were within ± 0.0005 inch (± 0.0013 cm). Unidirectional traverses were made in order to minimize errors due to gear play. Potential errors in displacement resulting from thermal distortion of the tip geometries and recording technique are expected to be within the values determined from the linearity of the actuators.

The output signals from both the pressure and temperature boundary-layer probes were monitored on the X-Y recorder.

DATA REDUCTION

Local Heat Flux

The local heat flux q was computed from the observed temperature gradient in the heat-flux meters. The temperature gradient in the meters can be described by the

Fourier conduction equation. The integrated form of this equation is

$$-qY = C_1 t^2 + C_2 t + C_3$$

The constants C_1 and C_2 were determined from a thermal-conductivity calibration of the Inconel specimen which was used to fabricate the heat-flux meters. The values of C_1 and C_2 are given in reference 10. The location Y of each Chromel-Alumel thermocouple on the heat-flux meter was determined by direct measurement. The unknowns q and C_3 were therefore determined by the simultaneous solution of two equations containing the measured temperature t and the corresponding location Y at two of the three measuring stations on the heat-flux meter. Wall temperatures were computed by setting $Y = 0$.

The heat-flux error considerations discussed in references 8 to 10 are also applicable to the present study. The principal error in the measured heat flux was due to the air gap around the heat-flux meter. The effect of the air gap was to increase the measured heat flux through local distortion of the wall temperature distribution. The uncertainty factor associated with this error in heat flux was estimated to be 10 percent; however, in this investigation all experimental heat-transfer results will be presented as computed from the direct measurements of one-dimensional heat flux.

The experimental values of throat heat transfer in the 30° nozzle, which were uncorrected for errors resulting from the air gap around the heat-flux meter, are in good agreement with the results of an independent investigation described in reference 11. The heat transfer was measured by a method which differed from that of the present study. Upon correcting the data of reference 11 for differences in contraction area ratio and gas-property evaluation technique, the agreement in throat heat transfer was within about 5 percent (see appendix A). The error in the measurements of reference 11 at high Reynolds numbers was about ± 8 percent. The good agreement in the results suggests that suitable accuracy can be obtained from the one-dimensional heat-transfer measurements of this investigation without applying corrections for air-gap effects.

Boundary-Layer Velocity Profiles

The kinetic-head measurements obtained with the boundary-layer stagnation-pressure probe were converted to velocities by means of the incompressible Bernoulli equation, which is

$$P_t - P_s = \frac{1}{2} \rho u^2 = P_t - P_w$$

The local density ρ evolved from the perfect gas law in which the measured wall static pressure and local stagnation temperature were the principal input. In this formulation, the local static pressure was assumed to equal the observed wall static pressure. The static temperature was assumed equal to the local stagnation temperature ($T_s = T_t$) because the maximum Mach number M at a survey station was quite low ($M \leq 0.08$).

The boundary-layer velocity profiles will be presented in terms of the velocity ratio u/u_∞ and a nondimensional distance parameter y/δ . The free-stream velocity u_∞ was determined from the maximum value of the kinetic-head measurements. Discussion of the method used to obtain the velocity boundary-layer thickness δ will be deferred until the profiles are presented in the section entitled RESULTS.

Boundary-Layer Temperature Profiles

The thermocouples in the temperature probes were referenced to the plenum temperature, and the resulting differential signal was recorded. In reducing the temperature data the assumptions of negligible probe heat losses and a temperature recovery factor of 1.0 were employed. The latter assumption is valid since probe measurements were limited to very low Mach numbers.

Boundary-layer temperature distributions will be presented in terms of the temperature-difference ratio $(T_t - T_w)/(T_0 - T_w)$ and a nondimensional distance parameter y/Δ . The thermal boundary-layer thickness Δ was equal to the distance from the wall corresponding to a temperature-difference ratio of 0.99.

RESULTS

Axisymmetric Acceleration Parameter

An axisymmetric acceleration parameter of the type discussed in reference 3 has been derived in appendix B. Incorporation into the integral momentum equation of (1) the empirical relation of reference 12 for the form factor H , wall shear stress τ_w , and pressure-gradient form parameter Γ , and (2) a critical Reynolds number for laminarization equal to that for forward transition on a flat plate ($Re_\theta = Re_{\theta, cr} = 360$) yielded the following expression for the axisymmetric acceleration parameter K_{ax} :

$$K_{ax} = \frac{\nu_\infty}{u_\infty^2} \frac{du_\infty}{dx} + 0.352 \frac{\nu_\infty}{u_\infty r} \frac{dr}{dx}$$

Since all tests were conducted at the same nominal stagnation temperature (970°R (539K)), the local values of K_{ax} in the nozzles were simply functions of the stagnation pressure and geometry. The values of K_{ax} were computed by assuming that the free-stream velocities were related to the experimental wall static pressures (ref. 10) through the isentropic relations for a perfect gas. A computer program used a spline-fit and numerical differentiation technique to calculate the derivatives of velocity and radius, du_{∞}/dx and dr/dx , respectively.

The local values of K_{ax} for the 30° and 60° nozzles are plotted in figures 3 and 4 as functions of the area ratio A/A^* . Distributions of K_{ax} are given for each value of the experimental stagnation pressure P_0 , which ranged from 2.0 to 20.4 atmospheres (2.03×10^5 to $20.67 \times 10^5\text{N/m}^2$). Figures 3 and 4 show that at fixed stagnation conditions the value of K_{ax} tends to decrease with decreasing area ratio, but at a given station K_{ax} increases with decreasing stagnation pressure.

A line representing the critical value of the axisymmetric acceleration parameter ($K_{ax,cr} = 2.88 \times 10^{-6}$, as derived in appendix B) is also shown in figures 3 and 4. The re-

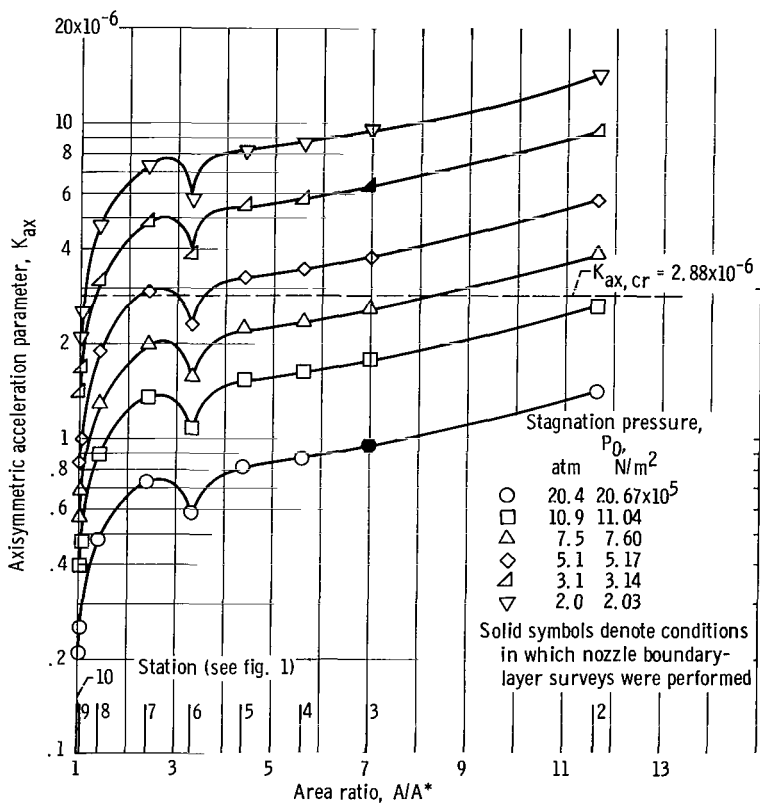


Figure 3. - Distribution of acceleration parameter in 30° nozzle computed for isentropic flow with measured wall static pressures. Nominal stagnation temperature, T_0 , 970°R (539K).

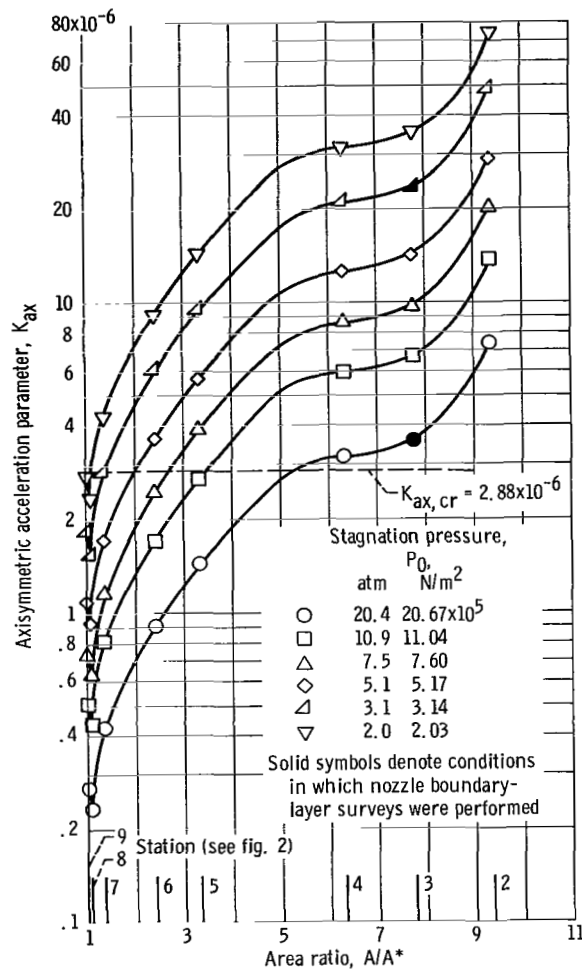


Figure 4. - Distribution of acceleration parameter in 60° nozzle computed for isentropic flow with measured wall static pressures. Nominal stagnation temperature, T_0 , 970° R (539 K).

sults of the derivation in appendix B indicate that for $K_{ax} < K_{ax, cr}$ the velocity boundary layer remains turbulent; however, for $K_{ax} > K_{ax, cr}$ the velocity boundary layer becomes laminar.

Although certain physical insight into the laminarization process associated with the velocity boundary layer can be gained from reference 7, it is difficult to comprehend the exact nature of the process in relation to the heat transfer in nozzles. The previous history of both the velocity and thermal layers is expected to appreciably influence the mechanisms governing the local transport of heat. Since the derivation of the acceleration parameter was based on the momentum equation only, the laminarization model essentially precludes the effects of a thermal boundary layer and the interaction between the thermal and momentum layers. The results of references 9 and 10 suggested that the in-

teraction between the layers might be weak. A knowledge of the thermal boundary layer (energy-calculation method) was sufficient to yield reasonably good predictions of nozzle heat transfer. In view of the possible importance of the thermal boundary layer, a straightforward application of the acceleration parameter in quantitatively assessing the nozzle heat transfer does not appear feasible.

Based on the laminarization criterion, the distributions of K_{ax} for the 30° nozzle (fig. 3) indicate that the velocity boundary layer at $P_0 = 20.4$ and 10.9 atmospheres (20.67×10^5 and 11.04×10^5 N/m²) should be characteristically turbulent. However, at $P_0 < 7.5$ atmospheres (7.60×10^5 N/m²), the velocity boundary layer should experience laminarization. The extent of the laminarization increases with decreasing pressure level. For instance, at $P_0 = 2.0$ atmospheres (2.03×10^5 N/m²), K_{ax} is greater than $K_{ax, cr}$ at all stations except in the vicinity of the throat. In this case a predominantly laminar boundary-layer history is expected to influence the heat exchange at the throat. Since history considerations cannot be dismissed, the throat values of K_{ax} which were less than $K_{ax, cr}$ do not necessarily imply the existence of a turbulent velocity boundary layer at the throat. This same argument can be applied to the distributions of K_{ax} for the 60° nozzle (fig. 4).

A comparison of the distributions of K_{ax} for the two nozzles (figs. 3 and 4) indicates that the steeper convergence angle of the 60° nozzle tends to induce laminarization over a wider range of conditions. This is most apparent at the highest stagnation pressures ($P_0 = 20.4$ and 10.9 atm; 20.67×10^5 and 11.04×10^5 N/m²). The results in figure 3 indicate that at these pressure levels the velocity boundary layer in the 30° nozzle will remain turbulent; however, laminarization can be expected in the 60° nozzle (fig. 4). At $P_0 = 20.4$ atmospheres (20.67×10^5 N/m²), values of $K_{ax} > K_{ax, cr}$ occur at three stations in the upstream portion of the 60° nozzle.

Boundary-layer surveys were obtained at the conditions designated by the shaded symbols in figures 3 and 4. The results of figures 3 and 4 for the 30° and 60° nozzles, respectively, indicate that a laminar-type velocity boundary layer should occur at $P_0 = 3.1$ atmospheres (3.14×10^5 N/m²) since $K_{ax} > K_{ax, cr}$. However, at $P_0 = 20.4$ atmospheres (20.67×10^5 N/m²) a turbulent velocity boundary layer would be expected for the 30° nozzle (fig. 3) since $K_{ax} < K_{ax, cr}$. According to figure 4, a laminar-type velocity boundary layer would be expected at the survey station in the 60° nozzle during high-stagnation-pressure operation. The observed nozzle velocity profiles at these two pressure levels were indeed consistent with the predictions for the 30° nozzle evolving from figure 3. The nozzle velocity boundary layer at $P_0 = 20.4$ atmospheres (20.67×10^5 N/m²) was similar in shape to turbulent pipe-flow profiles. The profile at $P_0 = 3.1$ atmospheres (3.14×10^5 N/m²) approached a type which is often associated with laminar flow. The velocity profiles in the 60° nozzle appeared to be of a laminar type at $P_0 = 3.1$ atmospheres (3.14×10^5 N/m²); however, at the high stagnation pressure the velocity pro-

file appeared to be more characteristic of a turbulent boundary layer. This result is not predictable on the basis of the K_{ax} distribution of figure 4. Further details concerning the observed boundary layer will follow the presentation of the heat transfer results.

Heat Transfer

The nozzle heat transfer will be presented in terms of the nondimensional grouping, $St_{ref}Pr^{0.7}$, given by the following equation:

$$St_{ref}Pr^{0.7} = \frac{q}{\rho_{ref}u_{\infty}(i_{ad} - i_w)} Pr^{0.7}$$

where the adiabatic enthalpy is given by

$$i_{ad} = i_s + Pr^{1/3}(i_0 - i_s)$$

The subscript *ref* denotes that properties were evaluated at the reference enthalpy condition given by

$$i_{ref} = i_s + 0.5(i_w - i_s) + 0.22 Pr^{1/3}(i_0 - i_s)$$

The Prandtl number *Pr* in the above relations was assumed to have a constant value of 0.71. The enthalpies were computed from the equations of reference 13 assuming an isentropic expansion process.

The experimental heat transfer will be compared to predicted values based on commonly used pipe-flow type of correlation equations for turbulent and laminar boundary layers which relate the heat transfer primarily to the Reynolds number based on the local diameter. The expressions used in this investigation take the form

$$St_{ref}Pr^{0.7} = 0.026 Re_{D,ref}^{-0.2} \tag{1}$$

for a turbulent boundary layer, and

$$St_{ref}Pr^{0.7} = 0.29 Re_{D,ref}^{-0.5} \tag{2}$$

for a laminar boundary layer. The Reynolds number $Re_{D,ref}$ based on the local diameter is given by

$$Re_{D,ref} = \frac{\rho_{ref} u_{\infty} D}{\mu_{ref}}$$

Experimental and predicted values of $St_{ref} Pr^{0.7}$ are presented as a function of $Re_{D,ref}$ for the 30° and 60° nozzles in figures 5 and 6, respectively. The experimental heat-transfer results were obtained at a nominal stagnation temperature of $970^{\circ}R$ (539 K) and stagnation pressures ranging from 2.0 to 20.4 atmospheres (2.03×10^5 to 20.67×10^5)

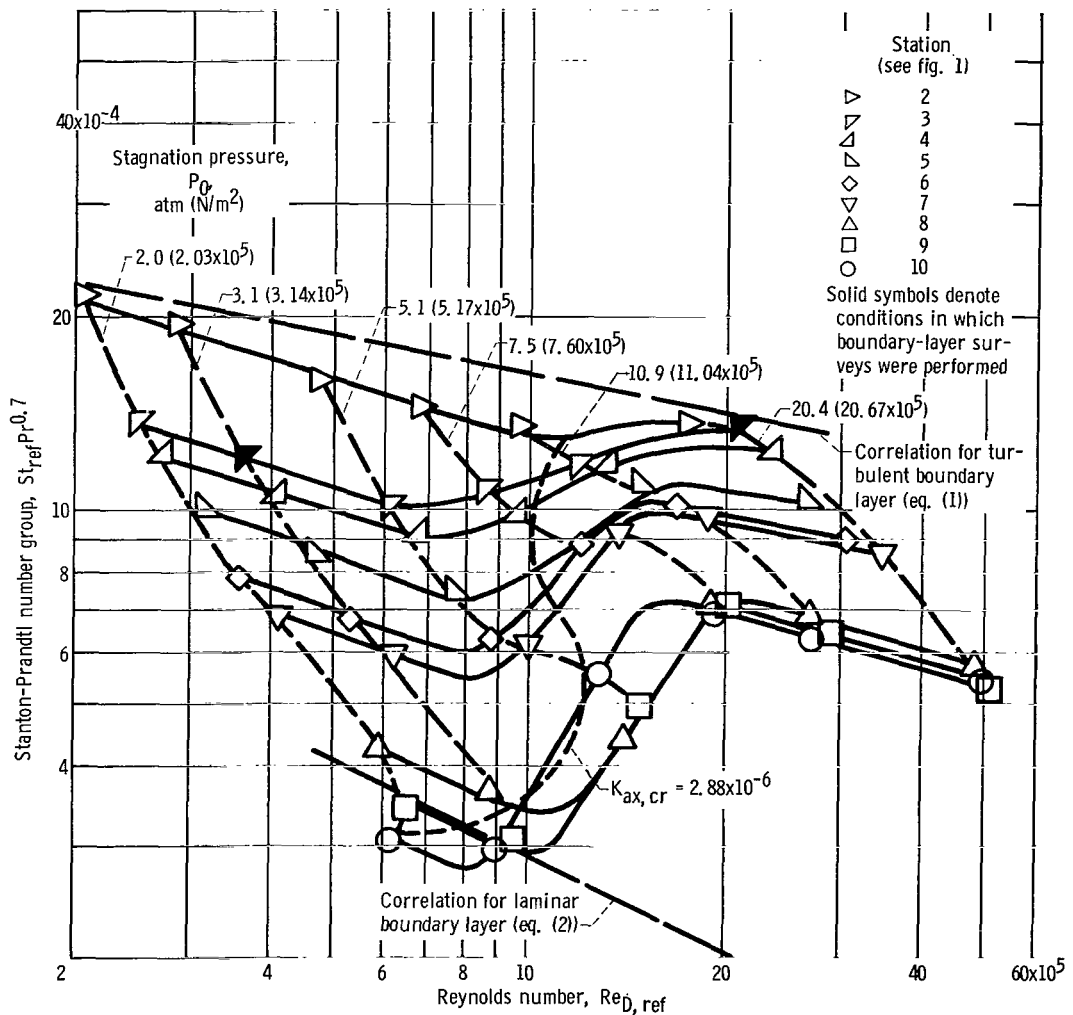


Figure 5. - Heat transfer as function of Reynolds number for various stations in 30° nozzle. Nominal stagnation temperature, T_0 , $970^{\circ}R$ (539 K).

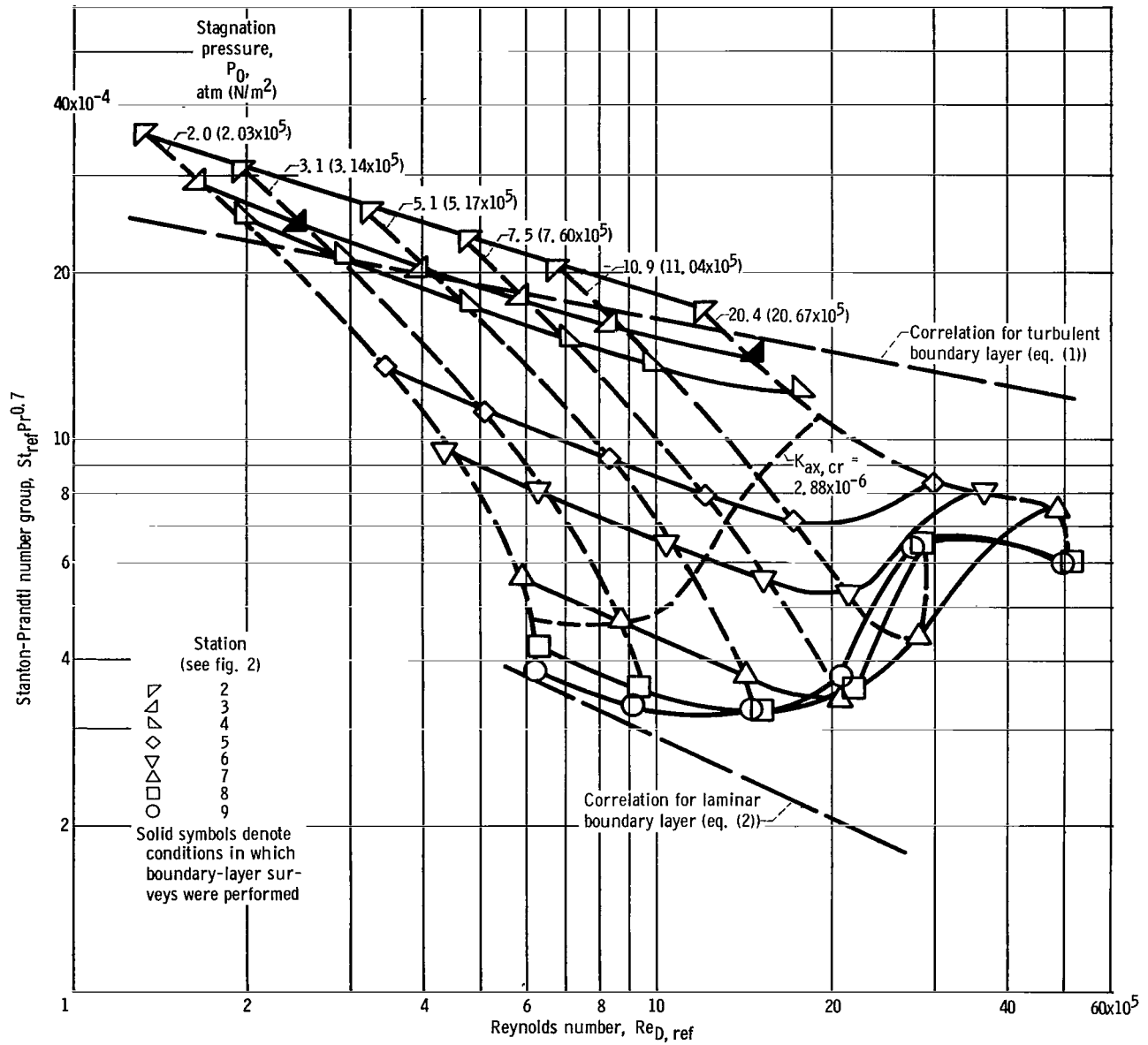


Figure 6. - Heat transfer as function of Reynolds number for various stations in 60° nozzle. Nominal stagnation temperature, T_0 , 970° R (539 K).

N/m^2). Experimental values of $St_{ref}Pr^{0.7}$ are presented for stations 2 to 10 in the 30° nozzle and for stations 2 to 9 in the 60° nozzle. Station 2 is located near the nozzle entrance and stations 9 and 10 correspond to the geometric throats in the 60° and 30° nozzles, respectively (refer to figs. 1 and 2). The lines of constant stagnation pressure, which have been cross plotted in figures 5 and 6, connect each of these stations in the nozzle and denote data which are consistent with a given test at the designated stagnation pressure.

The predicted heat transfer based on correlation equations (1) and (2) for turbulent and laminar boundary layers, respectively, merely provides an approximate upper and lower bound for the experimental values of $St_{ref}Pr^{0.7}$. The experimental heat transfer at a given station in each nozzle generally exhibits two distinct depressions from the predicted values based on the turbulent boundary-layer correlation. Exceptions to this result can be noted at stations 2, 3, and 4 in the 60° nozzle (fig. 6). The depression in heat transfer at a given station is lower at low Reynolds numbers or, in terms of a fixed Reynolds number, the depression is greatest in or near the throat of the nozzle. At high Reynolds numbers ($Re_{D,ref} \geq 2.0 \times 10^6$ and 3.0×10^6 for the 30° and 60° nozzle, respectively), the heat transfer at the throat is only about 50 percent of the values based on the turbulent boundary-layer correlation; however, the throat heat transfer, although appreciably reduced, is still about three times greater than predictions based on the laminar boundary-layer correlation (eq. (2)). The 60° nozzle throat heat transfer at the highest Reynolds numbers was about 13 percent greater than corresponding values in the 30° nozzle.

The throat heat transfer in the two nozzles at Reynolds numbers below about 10^6 was essentially equal to the predicted values based on the laminar boundary-layer correlation. The throat heat transfer in the 60° nozzle was about 20 percent higher than the values in the 30° nozzle. Figure 5 shows that, in the lower Reynolds number regime, the experimental heat transfer at the upstream station in the 30° nozzle was within -20 percent of the predictions based on the turbulent boundary-layer correlation; however, in progressing downstream the heat transfer approached the laminar values. In the 60° nozzle, the upstream heat transfer exceeded values based on the turbulent boundary-layer correlation by as much as 40 percent; however, as in the 30° nozzle, the heat transfer approached laminar levels near the throat. The high values of upstream heat transfer ($St_{ref}Pr^{0.7}$) in the 60° nozzle are attributed primarily to a velocity level which is lower in the nozzle entrance than one-dimensional (pipe flow) values. This reduced velocity is the result of abrupt turning at the entrance of the 60° nozzle. The use of one-dimensional values of velocity in the computation of $St_{ref}Pr^{0.7}$ and $Re_{D,ref}$ shifts the station 2 distribution in figure 6 to within a few percent of the predictions based on equation (1).

Laminarization of the boundary layer is believed to occur in the low Reynolds number range because the heat transfer, which was characteristic of a turbulent boundary layer

near the nozzle entrance, diminished to laminar levels at the throat. Evidence of laminarization in terms of time-mean boundary-layer surveys will be presented in the next section. The surveys were obtained at the conditions represented by the shaded symbols in figures 5 and 6.

A dashed line representing the locus of values of the critical acceleration parameter for axisymmetric flow ($K_{ax, cr} = 2.88 \times 10^{-6}$) is shown in figures 5 and 6. This line can be alternately interpreted as the locus of conditions in which the momentum-thickness Reynolds number attains the assumed critical value of 360. The line was established by linear interpolation and cross plotting of the results of figures 3 and 4 by means of the inverse relation between Reynolds number and the square root of the area ratio, which is given by

$$Re_D \propto \left(\sqrt{A/A^*} \right)^{-1}$$

This expression is valid for one-dimensional isentropic flow of a perfect gas at constant stagnation pressure, temperature, and dynamic viscosity. In cross plotting the results, Re_D was assumed equal to $Re_{D, ref}$.

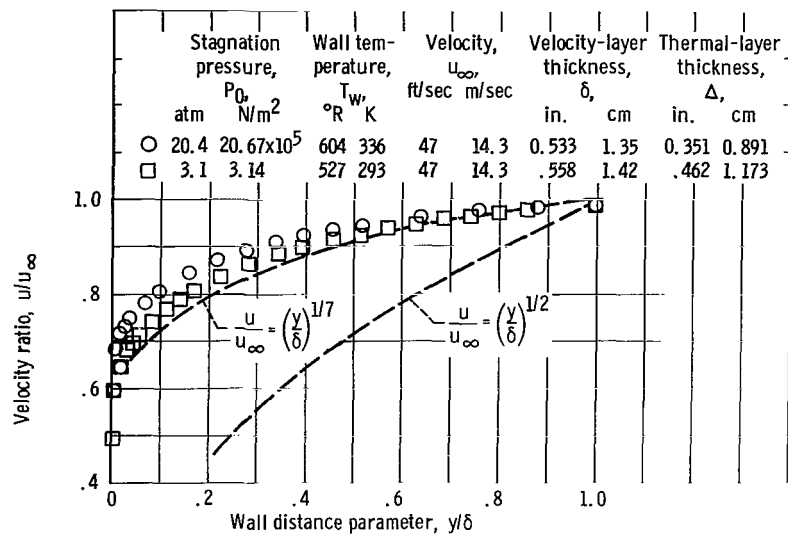
The dashed line in figures 5 and 6 corresponding to $K_{ax, cr} = 2.88 \times 10^{-6}$ can be interpreted with the aid of figures 3 and 4, respectively, as follows:

- (a) All data to the left of the line (lower Reynolds number range) reflect the influence of a laminarized velocity boundary layer ($K_{ax} > K_{ax, cr}$).
- (b) All data to the right of the line correspond to a turbulent velocity boundary layer ($K_{ax} < K_{ax, cr}$).

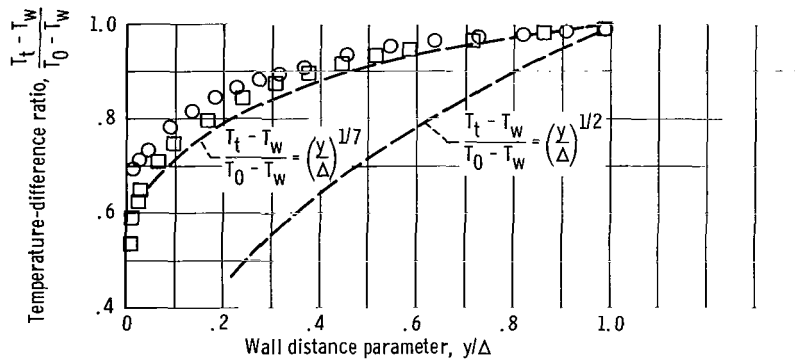
This dashed line in figures 5 and 6 establishes a fair definition of the regions of large depressions from the turbulent heat-transfer predictions at low Reynolds numbers and the much smaller depressions occurring at high Reynolds numbers. The greatest discrepancy between the experimental heat transfer and quantitative estimates emanating from figures 3 and 4 occurs in the throat region of the nozzles. Here the acceleration parameter was less than the critical value for all stagnation pressures (Reynolds numbers), thus suggesting a turbulent boundary layer locally. However, inspection of figures 5 and 6 reveals laminar levels of throat heat transfer. This discrepancy merely emphasizes the deficiencies in the laminarization model. As noted previously, these deficiencies involve both the boundary-layer history and the interaction between the thermal and momentum layers.

Boundary-Layer Profiles

The boundary-layer velocity and temperature profiles in the pipe inlet are presented



(a) Velocity profiles.



(b) Temperature profiles.

Figure 7. - Boundary-layer velocity and temperature profiles in pipe inlet.
Nominal stagnation temperature, T_0 , $970^{\circ}R$ ($539K$).

in figure 7. These surveys were obtained at a nominal stagnation temperature T_0 of $970^{\circ}R$ ($539K$) and stagnation pressure P_0 of 20.4 and 3.1 atmospheres (20.67×10^5 and $3.14 \times 10^5 N/m^2$). The experimental results are compared with profiles based on 1/7- and 1/2-power laws, which, as noted in reference 14, have been commonly used to classify the flow regime. In reference 14, velocity profiles having power laws of 1/2 to 1/11 were measured in favorable pressure gradient flows over a centerbody near Mach 1.0. The profiles, characterized by power laws in the range of 1/7 to 1/11, were associated with a turbulent boundary layer, whereas profiles having a power law of 1/2 were associated with a laminar boundary layer. In this investigation, the arbitrarily selected 1/7- and 1/2-power laws will be assumed to represent a turbulent and a laminar boundary layer, respectively, and will be used as a reference in the interpretation of the measured profiles.

A comparison of the velocity profiles of figure 7(a) and the temperature profiles of figure 7(b) with the 1/7-power law clearly indicates the presence of a turbulent boundary layer in the inlet at both the high (20.4 atm; $20.67 \times 10^5 \text{ N/m}^2$) and low (3.1 atm; $3.14 \times 10^5 \text{ N/m}^2$) stagnation pressure levels. These profiles were measured nearly two diameters upstream of the entrance of each nozzle (see figs. 1 and 2). Similar turbulent boundary-layer profiles presumably existed at the entrances of the nozzles since the inlet boundary layer developed in essentially a zero pressure gradient flow field. This conclusion concerning the nozzle-entrance boundary layer is in qualitative agreement with the experimental heat transfer at the upstream stations in each nozzle which nearly equaled or exceeded the levels based on the turbulent boundary-layer correlation (figs. 5 and 6).

The boundary-layer velocity profiles in the 30° and 60° nozzles have been plotted in logarithmic coordinates in figures 8 and 9, respectively. These profiles were measured

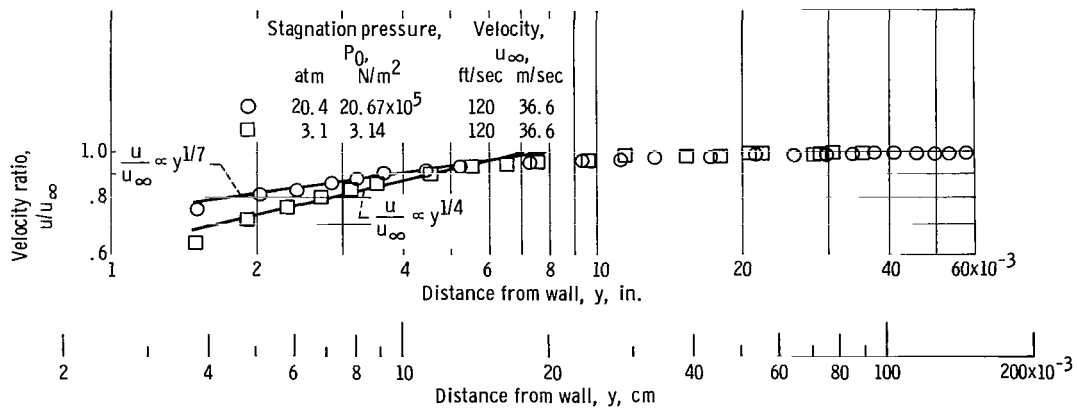


Figure 8. - Logarithmic plot of boundary-layer velocity profiles in 30° nozzle. Nominal stagnation temperature, T_0 , 970° R (539 K).

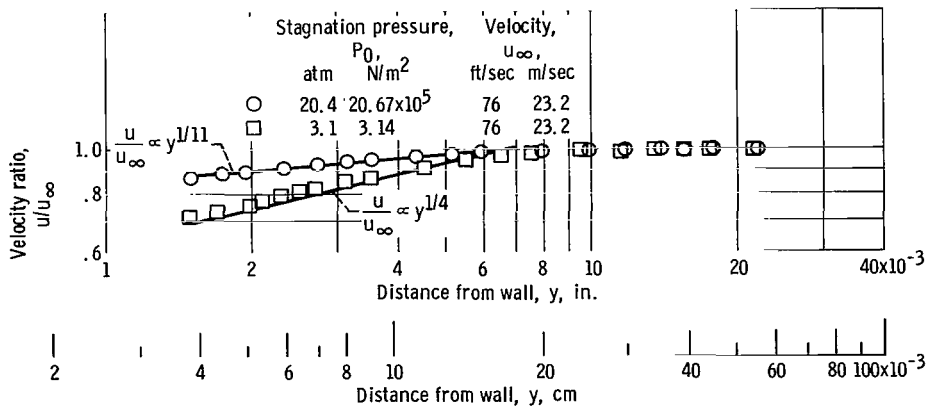


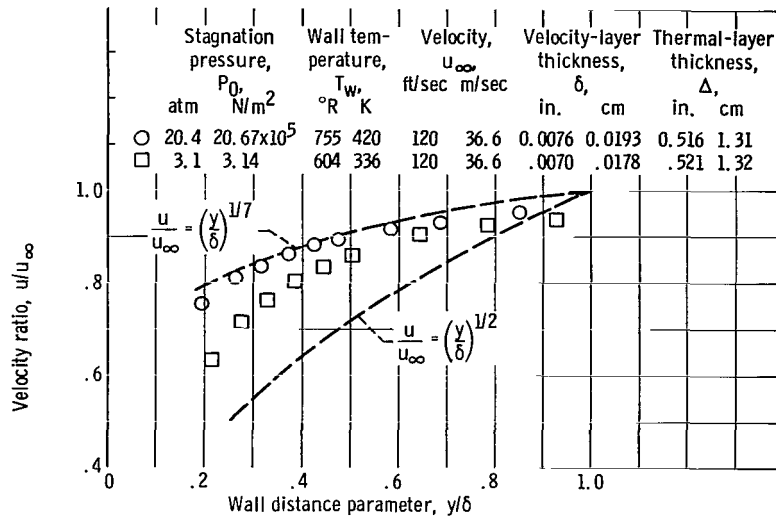
Figure 9. - Logarithmic plot of boundary-layer velocity profiles in 60° nozzle. Nominal stagnation temperature, T_0 , 970° R (539 K).

at the same stagnation conditions as the inlet boundary-layer surveys. The velocity profile at a stagnation pressure of 20.4 atmospheres ($20.67 \times 10^5 \text{ N/m}^2$) was nearly identical to the profiles reported in references 8 and 9, which were obtained under similar operating conditions. In references 8 and 9, an adiabatic rather than a cooled inlet was coupled to the present nozzle. It was noted in references 8 and 9 that the velocity boundary-layer thickness δ established in the conventional manner was quite ambiguous because of the flatness of the portion of the boundary layer extending from about 0.01 inch (0.025 cm) to the freestream. Futile attempts to correlate these profiles on the basis of a power law in which δ was selected in the outer "flat" portion of the profile resulted in the questioning of the power profile assumption when applied to nozzle flows. In the data of figures 8 and 9, only the portion of the boundary layer corresponding to y minus about 0.007 inch (0.0178 cm) can be correlated on the basis of a power law within the previously prescribed limits; however, the boundary layer appears to extend as far as $y \approx 0.06$ inch (0.152 cm) in the 30° nozzle and $y \approx 0.02$ inch (0.051 cm) in the 60° nozzle (figs. 8 and 9, respectively). The inner portion of the boundary layer at the high stagnation pressure (20.4 atm; $20.67 \times 10^5 \text{ N/m}^2$) appeared to correlate on the basis of 1/7- and 1/11-power laws corresponding to the 30° and 60° nozzles, respectively. At the low stagnation pressure (3.1 atm; $3.14 \times 10^5 \text{ N/m}^2$), the portion of the boundary layer in which $y < 0.007$ inch (0.0178 cm) can be correlated reasonably well on the basis of a 1/4-power law, but, again, the boundary layer may extend considerably beyond $y \approx 0.007$ inch (0.0178 cm).

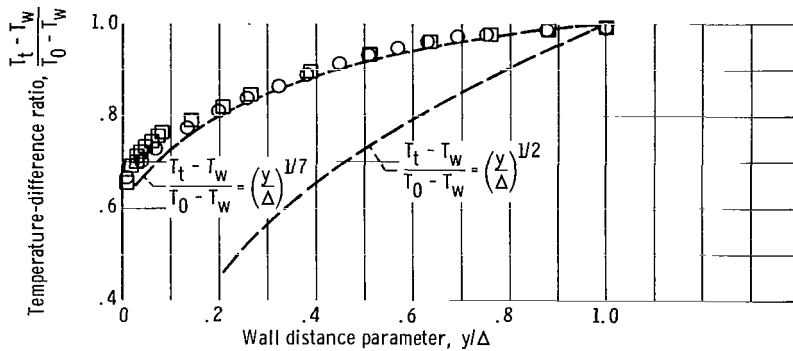
An unconventional assumption that has not yet been validated for nozzle-type flows is necessary in order to permit the analysis of these boundary layers on the basis of conventional power profiles. This assumption is to ignore the outer flow region completely, thus implying that the turbulent exchange mechanisms contributing to the production of shear at the wall are of predominant importance in the inner power-law portion of the boundary layer. The velocity boundary-layer thickness δ will, therefore, be determined by extrapolation of the inner part of the measured profile to $u/u_\infty = 0.99$ (figs. 8 and 9).

The boundary-layer velocity profiles in the 30° and 60° nozzles are plotted in rectangular coordinates in figures 10(a) and 11(a), respectively. The corresponding temperature profiles at the nozzle survey station are shown in figures 10(b) and 11(b). The velocity and temperature profiles in the two nozzles at the high stagnation pressure (20.4 atm; $20.67 \times 10^5 \text{ N/m}^2$) are essentially correlated by power laws in the range of 1/7 to 1/11, thus implying a turbulent boundary layer. Furthermore, the heat transfer at these conditions, denoted by the shaded symbols at $Re_{D, \text{ref}} = 2.1 \times 10^6$ and 1.5×10^6 (figs. 5 and 6, respectively), is in good agreement with the turbulent boundary-layer correlation.

The thermal boundary layer in the nozzles at the low stagnation pressure (3.1 atm; $3.14 \times 10^5 \text{ N/m}^2$) is also characteristic of a turbulent boundary layer as denoted by the correlation with a 1/7-power profile in figures 10(b) and 11(b). However, the velocity pro-



(a) Velocity profiles.



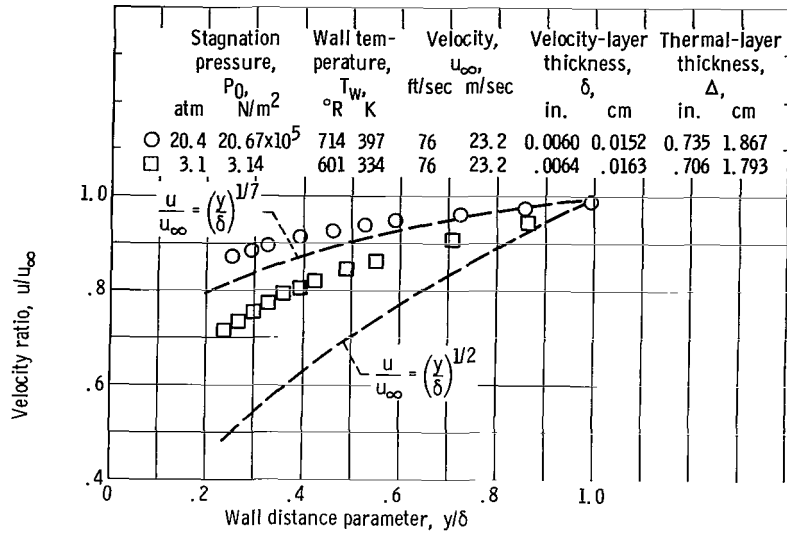
(b) Temperature profiles.

Figure 10. - Boundary-layer velocity and temperature profiles in 30° nozzle. Nominal stagnation temperature, T_0 , 970° R (539 K).

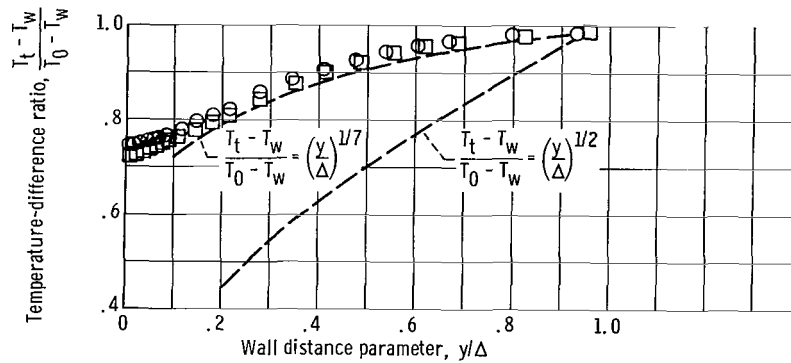
files, shown in figures 8, 9, 10(a), and 11(a), have been altered by the reduction in stagnation pressure. The profile lies between the 1/7-power turbulent and 1/2-power laminar profiles, thereby suggesting a transition towards the laminar-type boundary layer.

The heat transfer in the 30° nozzle corresponding to the conditions of the low-stagnation-pressure boundary-layer survey is denoted by the solid symbol at $Re_{D, ref} = 3.6 \times 10^5$ in figure 5. The heat transfer at the survey station was depressed to 60 percent of the value based on the turbulent boundary-layer correlation. In continuing along the line of constant stagnation pressure in figure 5, it can be noted that the throat heat transfer was in good agreement with predictions based on the laminar boundary-layer correlation.

The heat transfer at the boundary-layer survey station in the 60° nozzle is denoted by the solid symbols in figure 6 at $Re_{D, ref} = 2.4 \times 10^5$. In this case, a depression from the



(a) Velocity profiles.



(b) Temperature profiles.

Figure 11. - Boundary-layer velocity and temperature profiles in 60° nozzle. Nominal stagnation temperature, T_0 , $970^{\circ}R$ ($539K$).

predicted heat transfer for a turbulent boundary layer is not apparent at the survey stations; however, in progressing downstream along the line of constant stagnation pressure, the heat transfer approaches the laminar prediction.

It is interesting to note the relative thickness of the boundary layer in the inlet and nozzle at a given stagnation pressure (figs. 7, 10, and 11). In the inlet, the values of δ and Δ were comparable; in the nozzle, however, the velocity boundary layer was much thinner than the thermal boundary layer ($\delta \ll \Delta$). The thermal boundary layer between the survey stations in the inlet and nozzle was not significantly affected by the flow acceleration but thickened primarily because of increasing heat transfer and boundary-layer length. Considering the measured laminar-type velocity profile in the nozzles, the viscous dissipation is expected to be greatly reduced from that of the usually assumed turbulent $1/7$ -power velocity profile. Assuming this laminar-type velocity profile persists

at least to the nozzle throat, where the viscous dissipation is definitely a significant effect, the heat transfer can be greatly reduced.

DISCUSSION

The depressions from the predicted heat transfer based on the turbulent pipe flow type of correlation have been known to be associated with the reduction in turbulence intensity which accompanies flow acceleration. The results of this investigation support the feasibility of using a critical acceleration parameter $K_{ax, cr}$ to predict the regions of small and large depressions in the heat transfer. The value of $K_{ax, cr}$ (2.88×10^{-6}) is based primarily on the assumption that laminarization occurs at a critical momentum-thickness Reynolds number of 360, which is the classical value for forward transition on a flat plate.

In reference 3 it was noted that the depressions in heat transfer at high Reynolds numbers ($K_{ax} < K_{ax, cr}$) might be adequately accounted for by applying a correction factor involving K_{ax} to an energy-type prediction of the heat transfer. In reference 4, the application of a correction factor involving K_{ax} to data in which $K_{ax} < K_{ax, cr}$ resulted in a good prediction of the heat transfer in a two-dimensional nozzle. Unfortunately, the use of the acceleration parameter in predicting the highly depressed heat transfer at low Reynolds numbers is unknown. Therefore, caution should be exercised in applying laminar heat-transfer predictions to an initially turbulent flow even though $K_{ax} > K_{ax, cr}$. It has been demonstrated, however, that when $K_{ax} > K_{ax, cr}$ reductions in the normal levels of turbulent heat transfer can be expected.

SUMMARY OF RESULTS

Heat-transfer measurements were obtained in 30° and 60° half-angle of convergence nozzles at a nominal stagnation temperature of 970°R (539K) and over a range of stagnation pressures of about 2.0 to 20.4 atmospheres (2.03×10^5 to $20.67 \times 10^5 \text{N/m}^2$). These pressure levels provided throat Reynolds numbers based on diameter of about 6.0×10^5 to 5.0×10^6 . Additionally, time-mean boundary-layer velocity and temperature measurements were obtained at one station in a water-cooled pipe inlet and at a subsonic (Mach number ≤ 0.08) station in each nozzle at stagnation pressures of 3.1 and 20.4 atmospheres (3.14×10^5 and $20.67 \times 10^5 \text{N/m}^2$). The principal results of this study can be summarized as follows:

1. Inlet velocity and temperature profiles at the aforementioned stagnation pressure levels were characteristic of those for turbulent pipe flow; that is, the profiles were essentially described by a 1/7-power law. Although these measurements were obtained

nearly two diameters upstream of the nozzle, similar turbulent boundary-layer profiles were presumed to exist at the entrance of the nozzle.

2. The heat transfer at a given station in each nozzle generally exhibited two distinct depressions from predicted results based on a turbulent pipe-flow type of correlation. The smaller of the two depressions occurred at the higher Reynolds numbers where, in progressing downstream, the heat-transfer departure from predicted levels increased. At the throat of each nozzle, the heat transfer was about 50 percent of the predicted value.

A larger depression from the turbulent flow predictions of heat transfer occurred at the lower Reynolds numbers where there was evidence of laminarization of the initially turbulent velocity boundary layer. At these conditions, the throat heat transfer was approximately predictable by a laminar pipe-flow type of correlation.

The throat heat transfer in the 60° half-angle of convergence nozzle was about 13 percent higher than in the 30° half-angle of convergence nozzle at the highest Reynolds number, and it was about 20 percent higher at the lowest Reynolds number.

3. High Reynolds number ($Re_{D,ref} \approx 2.0 \times 10^6$) boundary-layer velocity and temperature surveys at a subsonic station in each nozzle yielded profiles which were essentially characteristic of turbulent pipe flow. The heat transfer at the survey station was within a few percent of the turbulent flow prediction.

Nozzle surveys at a lower stagnation pressure (3.1 atm ; $3.14 \times 10^5 \text{ N/m}^2$) revealed turbulent thermal boundary-layer profiles essentially described by a $1/7$ -power profile; however, the velocity profiles were of a laminar type corresponding to about a $1/4$ -power profile. Under these conditions the heat transfer at the survey station in the 30° half-angle of convergence nozzle was already depressed to 60 percent of the turbulent flow prediction; however, a depression in the survey-station heat transfer in the 60° half-angle of convergence nozzle was not apparent.

4. In progressing from the inlet to the survey station in each nozzle, the thermal boundary layer thickened; however, the velocity boundary layer diminished appreciably. Consequently, the thermal boundary layer at the nozzle survey station was much thicker than the velocity boundary layer.

5. A critical value of the axisymmetric acceleration parameter, derived from the integral momentum equation, provided a fair definition of the conditions in which the heat transfer was influenced by laminarization. The critical value of the axisymmetric acceleration parameter (2.88×10^{-6}) was based primarily on the assumption that laminarization occurs at a momentum-thickness Reynolds number of 360, which corresponds to the value for forward transition on a flat plate.

Lewis Research Center,
National Aeronautics and Space Administration,
Cleveland, Ohio, May 13, 1968,
129-01-11-04-22.

APPENDIX A

FURTHER CONSIDERATION OF ERROR IN EXPERIMENTAL HEAT TRANSFER

The predominant error in the experimental values of nozzle heat flux in this investigation was attributed to the air gap surrounding the plug. The purpose of this air gap was to allow for a one-dimensional transfer of heat in the plug which could be measured with a high degree of accuracy. In the following discussion, the results of these one-dimensional heat-flux measurements at the nozzle throat will be compared to the experimental heat-transfer results of reference 11 which were also obtained in a 30° half-angle of convergence nozzle having the same throat radius ratio ($r_c/r^* = 2.0$). Two important differences in the tests of reference 11 were (1) the nozzle heat transfer was measured by means of thermocouple plugs which were pressed into the wall, thus eliminating the air gap and (2) the nozzle contraction area ratio A_i/A^* was 7.75 compared to a value of 18.8 in the present investigation.

In order to account for the difference in A_i/A^* , additional tests were conducted with a 3.1-inch-diameter (7.87-cm-diam) by 18-inch-long (45.72-cm-long) water-cooled inlet ($A_i/A^* = 4.31$). In figure 12, the experimental throat heat-transfer results for these various configurations are compared with the data of reference 11 corrected for differences in the property evaluation technique. The predicted heat transfer based on the pipe-

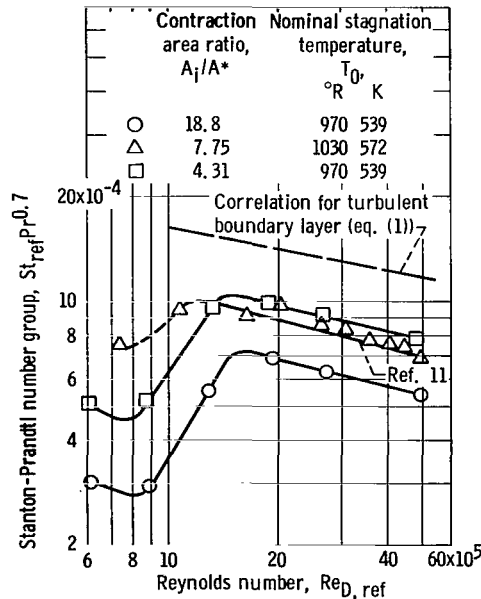


Figure 12. - Throat heat transfer of 30° nozzle as function of Reynolds number for various inlet-nozzle combinations.

flow type of correlation for a turbulent boundary layer is also presented since it approximately represents the upper limit of the throat heat transfer which would correspond to $A_i/A^* = 1.0$. It is important to note that this upper limit only applies to nozzles operating with cooled inlets of sufficient length to suppress the effects of step changes in wall temperature. The data of reference 9 show that in certain configurations the throat heat fluxes can exceed the values based on the correlation equation (eq. (1)) if a step change in wall temperature occurs at the nozzle entrance.

The throat heat transfer for the small contraction area ratio configuration ($A_i/A^* = 4.31$) is consistently higher than the values obtained in tests with the large contraction area ratio configuration ($A_i/A^* = 18.8$), as shown in figure 12. In the range of $2.0 \times 10^6 \leq Re_{D,ref} \leq 5.0 \times 10^6$, the results of reference 11 for $A_i/A^* = 7.75$ lie between the experimental values of this investigation, thus qualitatively indicating a consistent trend in the variation of throat heat transfer with A_i/A^* .

The variation of throat heat transfer with A_i/A^* for the above range of $Re_{D,ref}$ is given in figure 13. The throat heat transfer St_{ref}^* is made nondimensional by the predicted Stanton number based on the pipe-flow type of correlation $St_{ref,pf}$. In view of the curve faired through the average values of the throat heat transfer of the present study and the limiting value from the correlation equation, the heat-transfer results of reference 11 are greater by only about 5 percent. The good agreement in the results of these independent experiments suggests that the heat fluxes in this study, uncorrected for effects of the air gap, should provide an adequate representation of the true values.

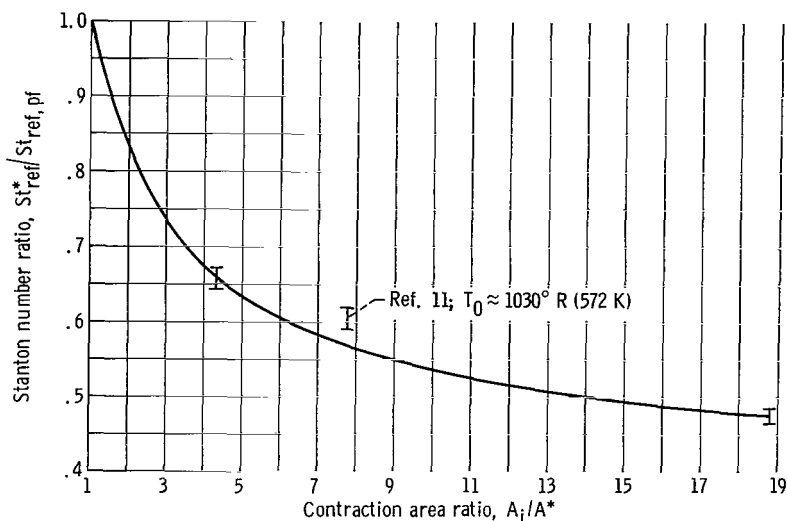


Figure 13. - Ratio of 30° nozzle throat heat transfer to pipe-flow prediction as function of contraction area ratio for $2 \times 10^6 \leq Re_{D,ref}^* \leq 5 \times 10^6$. Nominal stagnation temperature, T_0 , 970° R (539 K) unless specified.

APPENDIX B

AXISYMMETRIC ACCELERATION PARAMETER

In reference 3 an axisymmetric acceleration parameter was derived from the integral momentum equation. Flat-plate relations for the form factor and friction law were incorporated in the momentum equation in order to obtain the appropriate grouping of terms which are postulated to define the boundary conditions for laminarization of an initially turbulent boundary layer. In contrast to the analysis of reference 3, the following derivation will entail the use of the empirical relation of reference 12 for the shear stress, pressure gradient, and form factor. This relation, which was derived from experimental studies in an 8° half-angle of convergence conical nozzle, should be more applicable to the present investigation than the flat-plate empiricisms used in reference 3.

The integral momentum equation has the following form:

$$\frac{d\theta}{dx} + \left[\left(\frac{H+2}{u_\infty} \right) \frac{du_\infty}{dx} + \frac{1}{r} \frac{dr}{dx} + \frac{1}{\rho_\infty} \frac{d\rho_\infty}{dx} \right] \theta = \frac{\tau_w}{\rho_\infty u_\infty^2} \quad (\text{B1})$$

Multiplying equation (B1) by $\rho_\infty u_\infty / \mu_0$ and rearranging yields

$$\frac{d\text{Re}_\theta}{dx} + (H+1) \frac{\text{Re}_\theta}{u_\infty} \frac{du_\infty}{dx} + \frac{\text{Re}_\theta}{r} \frac{dr}{dx} = \frac{\tau_w}{\mu_0 u_\infty} \quad (\text{B2})$$

where the dynamic viscosity μ is assumed constant and equal to the viscosity at the stagnation temperature ($\mu = \mu_0$). In reference 12 a shear-stress parameter ϵ and the form factor $H = \delta^* / \theta$ were expressed as functions of a pressure-gradient parameter Γ , where ϵ and Γ are given by the following equations:

$$\epsilon = \frac{\tau_w}{\rho_\infty u_\infty^2} \text{Re}_\theta^{1/4} \quad (\text{B3})$$

$$\Gamma = \frac{\theta}{u_\infty} \frac{du_\infty}{dx} \text{Re}_\theta^{1/4} \quad (\text{B4})$$

Multiplication of equation (B2) by $\text{Re}_\theta^{1/4}$ and substitution of equations (B3) and (B4) gives the following alternate form of the momentum equation:

$$\frac{dRe_{\theta}^{5/4}}{dx} + \frac{5}{4} \frac{Re_{\theta}^{5/4}}{r} \frac{dr}{dx} = \frac{5}{4} \frac{\rho_{\infty} u_{\infty}}{\mu_0} [\epsilon - (H + 1)\Gamma] \quad (B5)$$

In reference 12 the bracketed group of terms on the right side of equation (B5) were found to be dependent on the pressure-gradient parameter Γ as shown by equation (B6).

$$\frac{5}{4} [\epsilon - (H + 1)\Gamma] = 0.016 - 3.55 \Gamma \quad (B6)$$

Substitution of equations (B6) and (B4) into equation (B5) yields the following equation for the momentum-thickness Reynolds number distribution in the nozzle:

$$\frac{dRe_{\theta}^{5/4}}{dx} + \frac{5}{4} \frac{Re_{\theta}^{5/4}}{r} \frac{dr}{dx} + 3.55 \frac{Re_{\theta}^{5/4}}{u_{\infty}} \frac{du_{\infty}}{dx} = 0.016 \frac{\rho_{\infty} u_{\infty}}{\mu_0} \quad (B7)$$

Equation (B7) can be readily solved for the change in Re_{θ} with distance x to give

$$\frac{dRe_{\theta}}{dx} = \frac{4}{5} \frac{u_{\infty}}{\nu_{\infty}} \left(\frac{0.016}{Re_{\theta}^{1/4}} - 3.55 Re_{\theta} \frac{\nu_{\infty}}{u_{\infty}^2} \frac{du_{\infty}}{dx} - \frac{5}{4} \frac{\nu_{\infty}}{u_{\infty}} \frac{Re_{\theta}}{r} \frac{dr}{dx} \right) \quad (B8)$$

In the highly accelerated flow in a nozzle, dRe_{θ}/dx attains a negative value, thus indicating a reduction in Re_{θ} with increasing distance x . If the value of Re_{θ} becomes sufficiently low, laminarization of the boundary layer is postulated to occur. The critical Reynolds number at which laminarization occurs will be assumed equal to the critical value for forward transition on a flat plate ($Re_{\theta, cr} = 360$). Substitution of $Re_{\theta, cr} = Re_{\theta} = 360$ into equation (B8) yields

$$\frac{dRe_{\theta}}{dx} = \frac{4}{5} \frac{u_{\infty}}{\nu_{\infty}} \left[0.00368 - 1278 \left(\frac{\nu_{\infty}}{u_{\infty}^2} \frac{du_{\infty}}{dx} + 0.352 \frac{\nu_{\infty}}{u_{\infty} r} \frac{dr}{dx} \right) \right] \quad (B9)$$

where the axisymmetric acceleration parameter K_{ax} is given by the terms in the inner brackets; that is,

$$K_{ax} = \frac{\nu_{\infty}}{u_{\infty}^2} \frac{du_{\infty}}{dx} + 0.352 \frac{\nu_{\infty}}{u_{\infty} r} \frac{dr}{dx} \quad (B10)$$

In order for laminarization to occur, the value of dRe_{θ}/dx at $Re_{\theta} = Re_{\theta, cr}$ must be less than zero. Consequently, the following inequality, derived from equation (B9), must be satisfied:

$$K_{ax} = \left(\frac{\nu_{\infty}}{u_{\infty}^2} \frac{du_{\infty}}{dx} + 0.352 \frac{\nu_{\infty}}{u_{\infty} r} \frac{dr}{dx} \right) > 2.88 \times 10^{-6} \quad (B11)$$

The critical value of the acceleration parameter is, therefore, given by

$$K_{ax, cr} = 2.88 \times 10^{-6} \quad (B12)$$

This value for the critical acceleration parameter is between the critical values used for the two-dimensional acceleration parameter $(\nu_{\infty}/u_{\infty}^2)(du_{\infty}/dx)$ in references 3 and 4.

REFERENCES

1. Back, L. H.; Massier, P. F.; and Cuffel, R. F.: Some Observations on Reduction of Turbulent Boundary-Layer Heat Transfer in Nozzles. *AIAA J.*, vol. 4, no. 12, Dec. 1966, pp. 2226-2229.
2. Launder, B. E.: Laminarization of the Turbulent Boundary Layer in a Severe Acceleration. *J. Appl. Mech.*, vol. 31, no. 4, Dec. 1964, pp. 707-708.
3. Moretti, P. M.; and Kays, W. M.: Heat Transfer Through an Incompressible Turbulent Boundary Layer With Varying Free-Stream Velocity and Varying Surface Temperature. Rep. No. PG-1, Thermosciences Div., Mech. Eng. Dept., Stanford Univ., Nov. 1964.
4. Back, L. H.; and Seban, R. A.: Flow and Heat Transfer in a Turbulent Boundary Layer With Large Acceleration Parameter. Proceedings of the 1967 Heat Transfer and Fluid Mechanics Institute. P. A. Libby, D. B. Olfe, and C. W. VanAtta, eds., Stanford Univ. Press, 1967, pp. 410-426.
5. O'Brien, R. L.; and Demarest, P. E.: Laminarization of Nozzle Wall Boundary Layers as a Means of Reducing Heat Flux. Rep. C910100-15, United Aircraft Corp., Oct. 1964. (Available from DDC as AD-460927.)
6. Talmor, E.: Sonic-Point Heat Transfer at Various Degrees of Upstream Acceleration. Paper No. 27, AIChE and ASME 9th National Heat Transfer Conference, Seattle, Wash., Aug. 6-9, 1967.
7. Schraub, F. A.; and Kline, S. J.: A Study of the Structure of the Turbulent Boundary Layer With and Without Longitudinal Pressure Gradients. Rep. No. MD-12, Thermosciences Div., Mech. Eng. Dept., Stanford Univ., Mar. 1965.
8. Boldman, Donald R.; Schmidt, James F.; and Fortini, Anthony: Turbulence, Heat-Transfer, and Boundary Layer Measurements in a Conical Nozzle With a Controlled Inlet Velocity Profile. NASA TN D-3221, 1966.
9. Boldman, D. R.; Schmidt, J. F.; and Ehlers, R. C.: Effect of Uncooled Inlet Length and Nozzle Convergence Angle on the Turbulent Boundary Layer and Heat-Transfer in Conical Nozzles Operating With Air. *J. Heat Transfer*, vol. 89, no. 4, Nov. 1967, pp. 341-350.
10. Boldman, Donald R.; Neumann, Harvey E.; and Schmidt, James F.: Heat Transfer in 30° and 60° Half-Angle of Convergence Nozzles With Various Diameter Uncooled Pipe Inlets. NASA TN D-4177, 1967.

11. Back, L. H.; Massier, P. F.; and Gier, H. L.: Convective Heat Transfer in a Convergent-Divergent Nozzle. Rep. TR-32-415, rev. 1, Jet Propulsion Lab., California Inst. Tech. (NASA CR-57326), Feb. 15, 1965.
12. Romanenko, P. N.; Leont'yev, A. I.; and Oblivin, A. N.: Investigation of Drag and Heat Transfer During Air Motion in Divergent and Convergent Nozzles. NASA TTF-11221, 1967.
13. McBride, Bonnie J.; Heimel, Sheldon; Ehlers, Janet G.; and Gordon, Sanford: Thermodynamic Properties to 6000⁰ K for 210 Substances Involving the First 18 Elements. NASA SP-3001, 1963.
14. Wesoky, Howard L.: Boundary-Layer Measurements in Accelerated Flows Near Mach 1. NASA TN D-3882, 1967.